Impingement of an Oblique Shock Wave on a Cylinder

C.M. Hung*
NASA Ames Research Center, Moffett Field, California

This paper presents a numerical simulation of impingement of an oblique shock wave on a cylinder. The study was undertaken to understand the three-dimensional shock wave and boundary-layer interactions occurring on problems such as the impingement of the bow shock wave from the Shuttle nose on an external tank, and store-carriage interference on a supersonic tactical aircraft. A thin-layer approximation of the Navier-Stokes equations is solved by a mixed explicit-implicit scheme for a supersonic Mach 4 flow with an incident shock angle of 25 deg. Both laminar and turbulent flows are investigated. Surface pressures show large extents of upstream influence, except near windward plane. Based on plots of velocity at the first mesh points above the cylinder body, a conjectured limiting-streamline pattern is constructed. Three-dimensional separation is studied, and the role of cross flow is discussed.

Nomenclature

A_1 = incident shock strength $= p_\infty / P_1$
A_2 = reflected shock strength $= p_2 / P_1$
D = diameter of cylinder
E = total energy $= e_i + 0.5(u^2 + v^2 + w^2)$
F,G,H = transport inviscid flux vectors, Eq. (1)
G_v = transport viscous flux vector, Eq. (1)
L = length of cylinder
M_∞ = freestream Mach number
M_1 = Mach number behind the oblique shock
p = static pressure $= (\gamma - 1)\rho e_i$
p_∞ = freestream static pressure
p_1 = static pressure behind oblique shock
p_N, p_2 = pressure after normal and regular oblique reflection
Re_D = Reynolds number based on diameter D
r = radial direction
$r_b(x), r_f(x), r_o(x)$ = radius of body, fine mesh, and outer coarse mesh, respectively
t = time
U = conservative variables $(\rho, \rho u, \rho v, \rho w, \rho E)$
u_∞ = freestream velocity
u,v,w = velocity in (x,r,ϕ) coordinates
v' = transformed velocity component $= v - r_b' u$
x = axial direction
X_1 = shock impingement point on $\phi = 0$ deg plane
α = angle of incident oblique shock wave
α_2 = angle of regular reflected shock wave
γ = ratio of specific heat = 1.4
(ξ,η,ϕ) = transformed cylindrical coordinates
ρ = density
$\sigma_{xx}, \sigma_{rx}, \sigma_{rr}, \sigma_{\phi\phi}, \sigma_{r\phi}, \sigma_{\phi x}$ = thin-layer approximated viscous terms
ϕ_x, ϕ_r = energy dissipation and diffusion terms

Presented as Paper 82-0025 at the AIAA 20th Aerospace Sciences Meeting, Orlando, Fla., Jan. 11-14, 1982; submitted Jan. 22, 1982; revision received May 3, 1982. This paper is declared a work of the U.S. Government and therefore is in the public domain.

*Research Scientist, Computational Fluid Dynamics Branch. Member AIAA.

Introduction

THE impingement of an oblique shock wave on a cylindrical-type geometry has a wide range of application in high-speed spacecraft design. Typical examples are impingement of the bow shock from the Shuttle nose on the wing leading edge, the wing shock on the external tank, and the store-carriage interference and separation on a supersonic tactical aircraft. The clean aerodynamic design often gives little consideration to the interference effect as well as the aerodynamic drag of the store-carriage. In practice, the induced drag, pressure, and heat loads may become a performance nightmare.

A planar oblique shock wave glancing through a cylinder is illustrated schematically in Fig. 1. The shock wave is reflected from the cylinder at various angles and strengths. The inviscid flowfield at each longitudinal location (as shown in Fig. 2) is very similar to that of planar shock-wave diffraction on a cylinder. Depending upon the freestream Mach number and the incident shock angle, the incident shock may be simply reflected at the first intersection with the cylinder (Fig. 2b). As the shock wraps itself around the cylinder, however, the simple reflection can no longer be sustained, and the reflection degenerates to a more complex λ, or even double λ structure (Figs. 2c and 2d), similar (but not identical) to the observation in shock-diffraction experiments.[1,2] At large incident angle there may exist no simple reflection for shock impingement, even at the first intersection with the cylinder. Then the flow structure at longitudinal locations near the first intersection with the cylinder has no similarity to those of the two-dimensional unsteady blast wave.

Due to the complexity, early theoretical studies[3] were concentrated on the prediction of inviscid properties for oblique reflection of shock waves at a rigid wall. These properties are highly significant in air blast applications. One finding of interest is that the head-on or normal reflection of a shock wave does not necessarily produce the strongest reflected shock wave. Oblique reflections result often in a stronger reflected shock wave and, hence, a higher peak pressure at the reflecting surface than for a normal reflection. Whitman[4,5] has presented an approximate theory for the dynamics of two- and three-dimensional shock waves, and has applied it to the description of shock diffraction on wedges and cones. Bryson and Gross[1] extended the Whitman theory to blunt two- and three-dimensional bodies, in particular, a

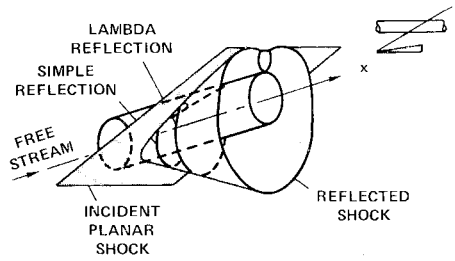

Fig. 1 Impingement of oblique shock on cylinder.

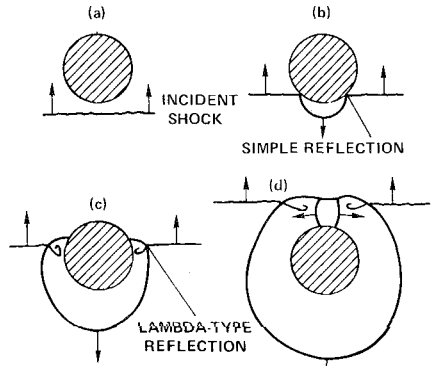

Fig. 2 Sketch of shock structure at various x locations.

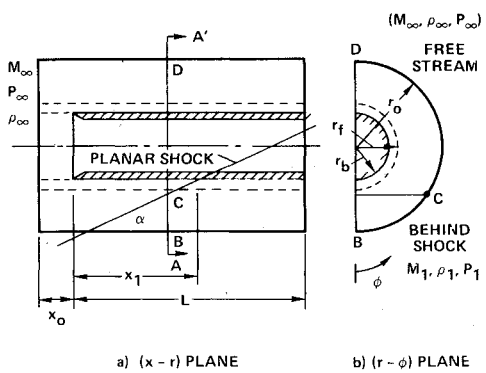

Fig. 3 Cross sections of the computational domain and the boundary conditions.

cylinder and a sphere. With the advent of high-speed computers and numerical schemes recently, there have been several inviscid calculations for shock-shock interaction and for blast wave-obstacle interaction.[6-8]

Holst[9] previously attempted to solve the full Navier-Stokes equations for three-dimensional shock-impingement problems. The main concern of his study was to investigate the intersection of the impinging shock with the bow shock wave on a blunt body, and calculations were carried out for strong shock waves and low Reynolds number flows.

In the present study, we modify the outer boundary conditions of a program previously developed for a general body of revolution.[10,11] The time-dependent, thin-layer approximation of the three-dimensional Navier-Stokes equations are solved by MacCormack's mixed explicit-implicit scheme[12] for supersonic flow over a hollow cylinder at zero incidence. The use of a hollow cylinder avoids the complication of prescribing the upstream incoming boundary conditions. The Reynolds number is high, and the leading-edge bow shock wave is weak and, hence, has insignificant effect on the main flowfield. The objectives of this study are to investigate three-dimensional impinging shock-wave and viscous boundary-layer interactions, and to examine the associated three-dimensional separated-flow structure.

A flow of freestream Mach number of 4 with an incident shock angle of 25 deg is studied. Both laminar and turbulent

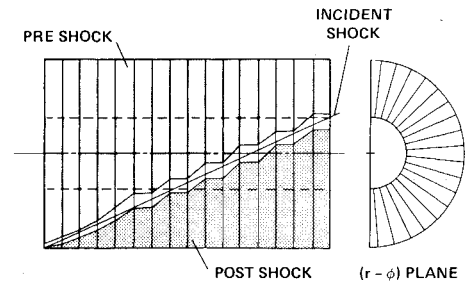

Fig. 4 Side view of the pre- and postshock wave location at the outer boundary.

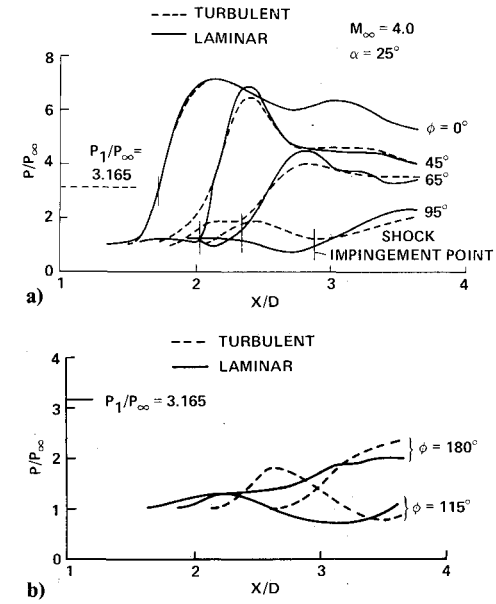

Fig. 5 Comparison of surface pressure for laminar and turbulent flow. a) ϕ from 0 to 95 deg; b) ϕ from 115 to 180 deg.

flows are calculated for a Reynolds number of 0.32×10^6, based on the cylinder diameter. The turbulent case may be considered as a result of tripping at the leading-edge region, and is used to demonstrate the effect of turbulence mixing on this interaction flowfield. Because of its similarity and relative simplicity, an inviscid result (code developed by Kutler and Fernquist[13]) of an "equivalent planar shock, or blast wave" over a cylinder will be used as a reference. It should be noted that we do not intend to study the detailed shock-wave structure of transition from a simple reflection to a more complicated λ reflection around the cylinder. Such a study is possible with the present method but would require more computer storage.

Analysis

Mesh System

Figure 3 shows the computational domains in the (x,r) and (r,ϕ) planes for a hollow cylinder. The flow is assumed to be symmetric in ϕ, and hence, only the half-plane 0 deg $\leq\phi\leq$ 180 deg is considered. The mesh spacings in the x, r, and ϕ directions may vary independently based on their own needs. In the present study, the mesh is uniformly spaced in both the x and ϕ directions. In the r direction a fine-mesh spacing is used in the region near the body, $r_b \leq r \leq r_f$, to resolve the viscous forces, and a coarse-mesh spacing is used in the outer region, $r_f \leq r \leq r_o$, where viscous effects are negligible. Both fine and coarse meshes are geometrically stretched.

Thin-Layer Approximation

The basic equations of the present analysis are the time-dependent compressible Navier-Stokes equations. For high Reynolds number flows, the viscous effects are confined to a

thin layer near the wall boundary and are dominated by the viscous term associated with the derivative in the r direction; consequently, all viscous terms associated with x and ϕ derivatives are neglected, while those with second derivatives in the r direction are retained. Written in weak conservative form in transformed cylindrical coordinates, the thin-layer approximation of the Navier-Stokes equations is as follows:

$$\frac{\partial rU}{\partial t}+\frac{\partial rF}{\partial \xi}+\frac{\partial r(G-G_v)}{\partial \eta}+\frac{\partial rH}{r\partial \phi}+Q=0 \qquad (1)$$

where

$$\xi=x$$

$$\eta=r-r_b(x)$$

$$v'=v-ur_b'(x)$$

and U represents the conservative variables, F, G, H are the transport inviscid fluxes, G_v is the thin-layer approximation of the transport viscous flux, and Q is the forcing term in the corresponding direction:

$$U=\begin{bmatrix}\rho\\ \rho u\\ \rho v\\ \rho w\\ \rho E\end{bmatrix} \quad F=\begin{bmatrix}\rho u\\ \rho u^2+p\\ \rho vu\\ \rho wu\\ (\rho E+p)u\end{bmatrix} \quad H=\begin{bmatrix}\rho w\\ \rho uw\\ \rho vw\\ \rho w^2+p\\ (\rho E+p)w\end{bmatrix}$$

$$G=\begin{bmatrix}\rho v'\\ \rho uv'-r_b'(x)p\\ \rho vv'+p\\ \rho wv'\\ (\rho E+p)v'\end{bmatrix} \quad G_v=\begin{bmatrix}0\\ \sigma_{rx}-r_b'(x)\sigma_{xx}\\ \sigma_{rr}-r_b'(x)\sigma_{rx}\\ \sigma_{r\phi}-r_b'(x)\sigma_{\phi x}\\ \Phi_r-r_b'(x)\Phi_x\end{bmatrix}$$

$$Q=\begin{bmatrix}0\\ 0\\ -p-\rho w^2+\sigma_{\phi\phi}\\ \rho vw-\sigma_{r\phi}\\ 0\end{bmatrix}$$

In the above equations, u,v,w are the velocity components in the axial, radial, and azimuthal x,r,ϕ directions; ρ, p, and E are density, pressure, and total specific energy, respectively; and $\sigma_{xx},\sigma_{rr},\sigma_{\phi\phi},\sigma_{rx},\sigma_{r\phi},\sigma_{\phi x}$, and Φ_x,Φ_r denote the thin-layer approximations of the viscous normal and shear stresses and heat flux components. The perfect gas relation is used and the molecular viscosity is evaluated by Sutherland's formula.

The above system of Eq. (1) is valid for turbulent as well as for laminar flow by replacing the molecular transport coefficients with their turbulent counterparts. A two-layer turbulence model developed by Baldwin and Lomax[14] is employed as a closure. The numerical technique used in this investigation is a mixed explicit-implicit scheme developed by MacCormack.[12] The scheme is second-order accurate in both time and space and captures the shock wave itself as the flowfield progresses from an arbitrary initial condition to an asymptotic steady state. The program is coded for treatment of a general body of revolution, i.e., $r_b=f(x)$, and has been used to calculate supersonic flows over cylinders with flared aft body at various angles of attack.[10,11] In the present calculation $r_b'(x)=0$, and the geometry is reduced to a perfect circular cylinder. Details of the numerical procedure are described in Refs. 10 and 11.

Boundary Conditions

The upstream boundary conditions can be either prescribed from a previous calculation, or, as shown in Fig. 3, that the upstream boundary is placed ahead of the leading edge of the hollow cylinder and the incoming flow is assumed to be uniform at supersonic freestream conditions $(M_\infty,p_\infty,\rho_\infty)$. A symmetry condition is applied at the $\phi=0$ and 180 deg planes, and a zero-gradient boundary condition is used at the downstream boundary. The wall is assumed impermeable and no-slip boundary conditions are used. The wall is taken to be either isothermal or adiabatic and the wall pressure is evaluated using $\partial p/\partial r=0$ at $r=r_b$. In the present case, the first mesh point is so close to the wall that this pressure condition is appropriate.

The impinging planar shock wave strikes the cylinder at an angle α, and intercepts on the windward plane, $\phi=0$ deg at X_I. To impose this shock impingement, the outer boundary conditions are set at freestream conditions $(M_\infty,p_\infty,\rho_\infty)$, ahead of the shock, C-D, and at postshock conditions (M_1,p_1,ρ_1), behind the oblique shock, B-C, as shown at cut A-A' in Fig. 3. This sounds simple and straightforward, but in a finite-difference application, with uniform mesh spacings in the x and ϕ directions, the interior mesh point will "see" the incident shock wave as a jagged surface, not a plane. This can be illustrated in a projected side view of the pre- and postshock-wave location imposed around the outer boundary (Fig. 4). It is well known that planar shocks are stable; that is, if a shock is disturbed from plane shape, the disturbance decays and the shock restores the plane shape as it propagates. The zigzag of the imposed shock wave will lead to dispersion and oscillation of the shock wave as the interior points try to "capture" it by the numerical scheme itself. It becomes more and more severe as the shock wraps around the cylinder, because the zigzag of the imposed shock wave is getting worse as ϕ increases, and furthermore, the induced error only propagates downstream in a supersonic flow. Details of this problem will be shown later. A simple remedy is to increase the mesh resolution with proper distribution of mesh point in the ϕ direction. However, an increase in mesh points is beyond the capability of the current computer, CDC 7600, and is not investigated here.

Results and Discussions

The case for Mach number $=4.0$ and Reynolds number $=0.32\times10^6$ based on a cylinder diameter of 101.6 mm was studied. The wall is assumed adiabatic, and both laminar and turbulent flows are calculated. The case of turbulent flow is considered as a result of tripping at the leading-edge region. A grid of $(45\times34\times20)$ encloses a computational domain of x/D from -0.225 to 3.735, $(r-r_b)/D$ from 0 to 0.909, and ϕ from -5 to 185 deg. A geometrically stretched fine mesh (20 points) in the r direction is used near the body up to $(r-r_b)/D=0.054$ with a minimum mesh spacing small enough to insure sufficient resolution in the laminar sublayer for the turbulent case. The incident shock wave with angle $\alpha=25$ deg (shock strength $p_1/p_\infty=3.165$), impinges on the most windward plane $\phi=0$ deg at $X_I/D=1.725$.

In this section numerical results are presented for pressure on the body surface, the pressure field at various longitudinal planes, and velocity plots very near the wall that represent the skin-friction lines on the body surface for the study of the separation pattern.

Figure 5 shows plots of surface-pressure distributions for $\phi=0$, 45, 65, 95, 115, and 180 deg (note the fine scale in Fig. 5b), and for both laminar and turbulent flows. The inviscid

shock jump and the shock impingement locations are indicated. The peak of pressure rise decreases gradually from more than two times of incident-shock jump on windward side down to less than the inviscid shock stength as ϕ greater than 90 deg. For $\phi = 0$ deg, the pressures for both laminar and turbulent cases are so close that they are almost indistinguishable. For larger ϕ, the pressures differ substantially. For laminar flow, the upstream influence extends way ahead of the shock-impingement point, but the pressure-rise plateau is very small. While for the turbulent flow, the upstream extent is relatively smaller, but the level of pressure rise is higher, compared with the laminar results. The cross flow, driven by the upstream pressure rise ahead of the inviscid shock, expands as it wraps over $\phi = 90$ deg and, hence, leads to pressures lower than the freestream value, as shown at $\phi = 95$ and 115 deg.

The first-order approximation to this problem is the solution for a blast shock wave with equivalent shock strength, $M_s = M_\infty \sin\alpha = 1.65$, over a cylinder. A calculation was carried out using a program developed by Kutler and Fernquist.[13] Figure 6 shows comparisons of surface pressures for laminar flow and the inviscid blast-wave solution. (The time history of pressure has been converted into longitudinal pressure profile.) The indicated normal reflection pressure level is

$$\frac{p_N}{p_\infty} = \frac{(2\Lambda^2+1)-\Lambda^2 A_1}{A_1(\Lambda^2+A_1)}$$

and the oblique reflected pressure, p_2/p_∞, is calculated from the following two relations[15]:

$$m = \frac{(1-A_1)\beta_1}{1+\Lambda^2 A_1+(A_1+\Lambda^2)\beta_1^2} = \frac{(A_2-1)\beta_2}{1+\Lambda^2 A_2+(A_2+\Lambda^2)\beta_2^2}$$

$$m^2(1-\Lambda^2)^2(\beta_1-\beta_2)+m[(1-\Lambda^2)^2-(\beta_1-\beta_2)^2 - (\Lambda^2+\beta_1\beta_2)^2]-(\beta_1-\beta_2)=0$$

where

$$\Lambda^2=\frac{\gamma-1}{\gamma+1} \quad A_1=\frac{p_\infty}{p_1} \quad A_2=\frac{p_2}{p_1} \quad \beta_1=\tan\alpha \quad \beta_2=\tan\alpha_2$$

Inclusion of viscous effects makes the pressure rise gradually. Otherwise, for small ϕ, the surface pressure from the inviscid and viscous solutions is in good qualitative agreement by taking into account the correction from blast-wave reflection to oblique-shock reflection. But as ϕ increases, mainly due to the cross-flow expansion driven by the upstream pressure rise, the pressure distribution becomes quite different from that of the inviscid blast-wave solution.

Figure 7 shows complete three-dimensional plots of surface pressure for both laminar and turbulent cases. Here again we can see the differences in upstream influence and the level of plateau pressure, for flows with and without the turbulent mixing.

Figures 8 and 9 show velocity plots of the first mesh points above the body surface at three projection views for laminar and turbulent flows, respectively. These plots represent the direction and magnitude of the surface skin friction, and are similar to the so-called "limiting streamlines." It is interesting to note that in the present turbulent case the so-called "streamwise separation line" shows no sign of u-velocity reversal, except near $\phi = 0$ and 180 deg; indeed, it only shows strong convergence, or coalition of skin-friction lines. The effects of turbulent mixing can be demonstrated clearly in the difference between Figs. 8a and 9a. The laminar case shows a large upstream influence, not present in the turbulent case, and also a much larger extent of cross-flow separation.

Figures 10a-c show unwrapped (u-w) velocity plots at three radial locations for laminar case. The solid lines represent the

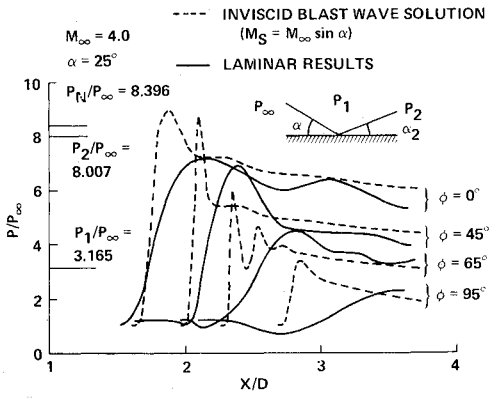

Fig. 6 Comparison of laminar solution with blast wave solution.

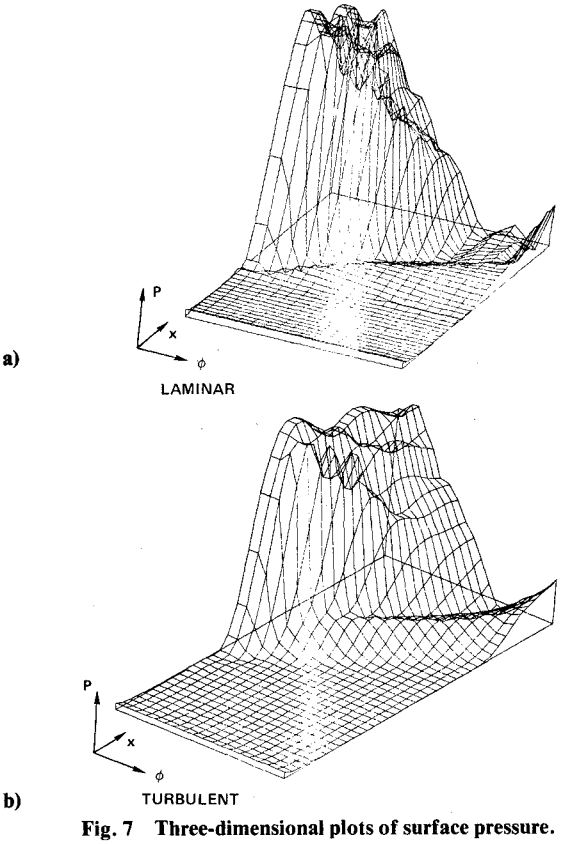

Fig. 7 Three-dimensional plots of surface pressure.

location of the inviscid shock wave. The complexity of Fig. 10a is astonishing. There seem to be five distinct regions as marked. Based on Figs. 8 and 10, a skin-friction pattern is conjectured as shown in Fig. 11 where S stands for saddle point, N for nodal point, N_s for nodal-point separation, and N_a for nodal-point reattachment. Figure 11a corresponds to Fig. 10a and Fig. 11b to Fig. 8a. Note that region III is part of region IV. Basically, two kinds of cross flow occur; the first one is imposed by the oblique shock, behaving as an "angle of attack" to the cylinder, and the second one is induced by the pressure gradient around the circumference. The second cross flow can be further subdivided into two: first a weak cross flow induced by the plateau pressure, and then a strong cross flow driven under sharp pressure rise. The appearance of region III is a result of change from a weak cross flow to a strong one. Ahead of the shock-wave and boundary-layer interaction, the boundary layer is uniform around the cylinder. The cross flow, at first induced by the plateau pressure and then by the sharp pressure rise and the imposed inviscid flow, convects fluid from windward to leeward. This leads to a thin boundary layer on the windward and a thick

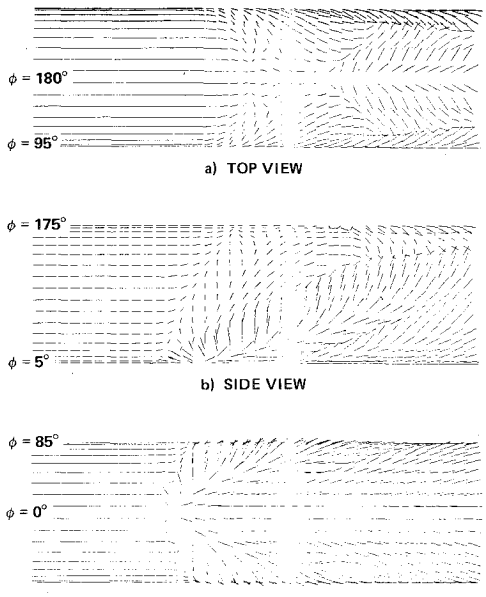

Fig. 8 Projection view of velocity vectors near body laminar.

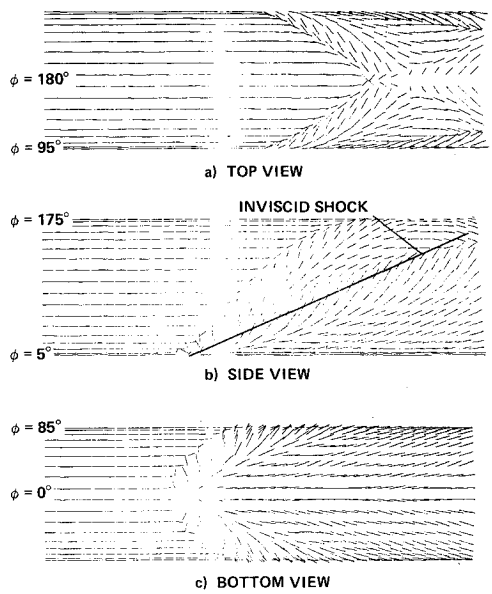

Fig. 9 Projections of velocity vectors near body surface—turbulent.

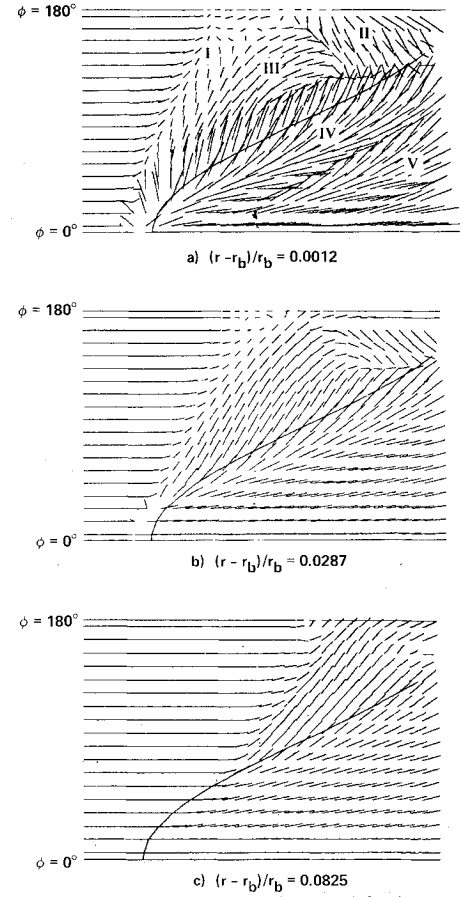

Fig. 10 Unwrapped velocity plots (u and w) for laminar plot.

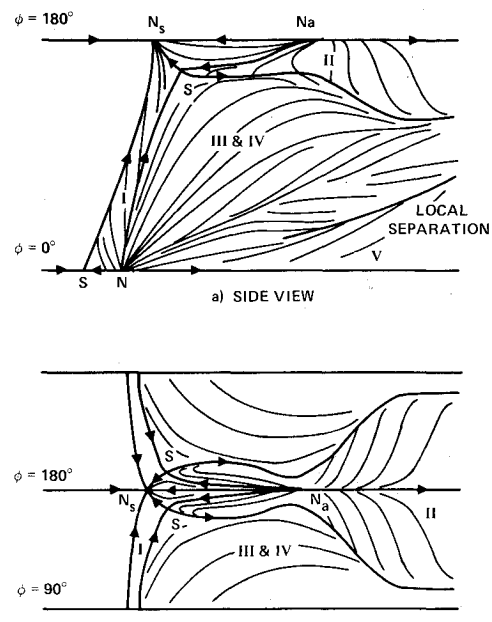

Fig. 11 Conjectured skin friction line development—laminar.

boundary layer on the leeward, which results in a small upstream influence around $\phi = 0$ deg, and large, elsewhere. The mechanism to balance or to damp out the momentum convected with the cross flow is very weak and often ends up with a pressure rise around $\phi = 180$ deg far upstream of the impingement of the oblique shock wave. The gradual rise of pressure around $\phi = 180$ deg then drives fluid away and leads to cross flow separation. Behind the impingement of the oblique shock, there shows a trace of skin-friction convergence, between regions IV and V, referred to as a "local separation." This is the result of a sharp pressure decrease after it reaches the peak, typically observed in a cylindrical shock reflection. Depending upon shock strength, the skin friction may show some degree of convergence but the flow may not separate.

Applying an advanced graphics technique, Figs. 12 and 13 show sequences of pressure fields at various x locations for both laminar and turbulent flows. Details of the shock wave encountering with, wrapping around, and reflecting from the cylinder are clearly shown and the existence of low pressure behind $\phi = 90$ deg, followed by a pressure buildup around $\phi = 180$ deg, is also clearly observed. Comparisons of laminar and turbulent results show a strong similarity of pressures on the windward side and a large deviation on the leeward side.

Since the incident shock wave has not been imposed in a planar sense, as discussed in the previous section, the dispersion of the pressure field occurs behind the shock wave. This is clearly shown in these sequences of pictures. In fact, in Fig. 12f (or Fig. 13f), a zigzag in the shock wave near the outer boundary is observed.

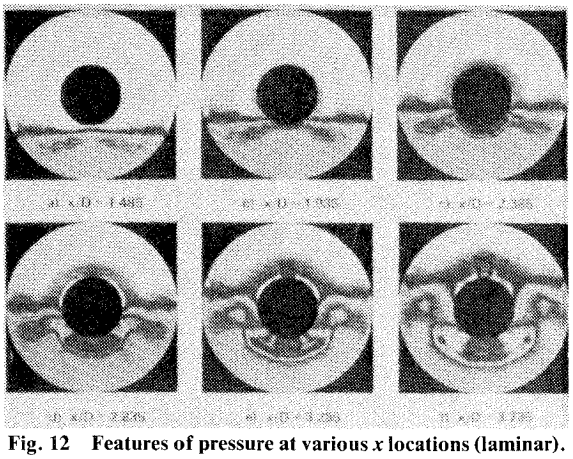

Fig. 12 Features of pressure at various x locations (laminar).

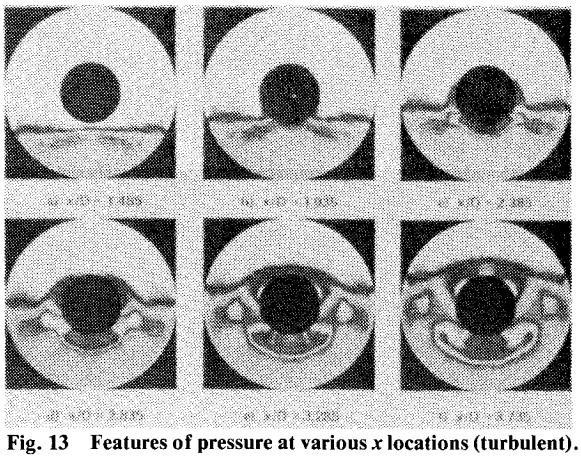

Fig. 13 Features of pressure at various x locations (turbulent).

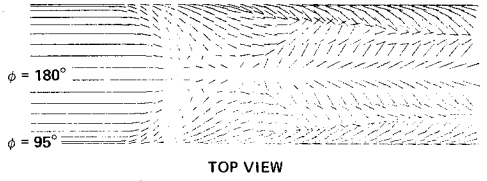

Fig. 14 Top view of velocity vectors near body surface for $x/D = 1.095$—laminar.

As indicated in Figs. 8 and 9, the computational domain is cut off before the incident shock completely glances through the cylinder. A case of shock impinging on the most windward plane, $\phi = 0$ deg at $X_I/D = 1.095$ (compared to the previous case of $X_I/D = 1.725$), has been calculated. The result (Fig. 14) is very similar to the previous calculation (Fig. 8c) in that the basic flow structure does not change, except where the cross-flow separation is well established as the shock wave completely wraps around the body.

Concluding Remarks

Impingement of an oblique shock wave on a cylinder has been numerically simulated. The time-dependent Navier-Stokes equations, with the thin-layer approximation, were solved by a mixed explicit-implicit numerical scheme. Both laminar and turbulent flows were investigated. For laminar flow, the extent of upstream influence is very large, except near the windward plane, but the level of plateau pressure is very low. Conversely, for turbulent flow, the upstream extent is smaller, but the level of plateau pressure is higher compared with the laminar results. The existence of turbulent mixing does not affect the flowfield very much on the windward side, but makes the results substantially different for ϕ bigger than 90 deg. The cross flow convects fluid from the windward to leeward and causes a gradual pressure rise well ahead of the inviscid shock, which in turn drives the flow away from leeward and leads to cross-flow separation. To establish a more planar oblique shock, imposed around the outer boundary, high-mesh resolution with clustering in the circumferential direction is necessary.

The three-dimensional program is coded in such a way as to permit treatment of a general body of revolution at angle of attack. The incident shock wave may be prescribed with curvature to resemble the bow shock generated from an arbitrary nose shape. Furthermore, the location of shock impingement can be a function of time to simulate an unsteady shock-wave impingement. Experimental measurements are needed to verify the numerical results and to confirm the present numerical observations.

References

[1] Bryson, A.E. and Gross, R.W.F., "Diffraction of Strong Shock by Cones, Cylinders, and Spheres," *Journal of Fluid Mechanics,* Vol. 10, Pt. 1, Feb. 1961, pp. 1-16.

[2] Heilig, W.H., "Diffraction of a Shock Wave by a Cylinder," *Physics of Fluids,* Supplement I, Vol. 12, May 1969, p. I-154-I-157.

[3] Polacheh, H. and Seeger, R.J., "Shock Wave Interaction," in *Fundamentals of Gas Dynamics,* edited by H.W. Emmons, Princeton University Press, Princeton, N.J., 1958, pp. 448-504.

[4] Whitman, G.B., "A New Approach to Problem of Shock Dynamics: Part I. Two-Dimensional Problems," *Journal of Fluid Mechanics,* Vol. 2, Pt. 2, March 1957, pp. 145-171.

[5] Whitman, G.B., "A New Approach to Problem of Shock Dynamics: Part II. Three-Dimensional Problems," *Journal of Fluid Mechanics,* Vol. 5, Pt. 3, April 1959, pp. 369-386.

[6] Kutler, P. and Shankar, V.S.V., "Diffraction of a Shock Wave by a Compression Corner: Part I. Regular Reflection," *AIAA Journal,* Vol. 15, Feb. 1972, pp. 197-203.

[7] Kutler, P. and Sakell, L., "Three-Dimensional Shock-on-Shock Interaction Problem," *AIAA Journal,* Vol. 13, Oct. 1970, pp. 1360-1367.

[8] Champney, J.M., Chaussee, D.S., and Kutler, P., "Computation of Blast Wave-Obstacle Interactions," AIAA Paper 82-0227, Jan. 1982.

[9] Holst, T.L., "Numerical Computation of Three-Dimensional Blunt Body Flow Fields with an Impinging Shock," Ph.D. Thesis, Iowa State University, Ames, Iowa, 1975.

[10] Hung, C.M., "Numerical Solution of Supersonic Laminar Flow Over an Inclined Body of Revolution," *AIAA Journal,* Vol. 18, Aug. 1980, pp. 921-928.

[11] Hung, C.M. and Chaussee, D.S., "Computation of Supersonic Turbulent Flows Over an Inclined Ogive-Cylinder-Flare," *AIAA Journal,* Vol. 19, Sept. 1981, pp. 1139-1144.

[12] MacCormack, R.W., "An Efficient Numerical Method for Solving the Time-Dependent Compressible Navier-Stokes Equations at High Reynolds Number," NASA TM X-73129, July 1976.

[13] Kutler, P. and Fernquist, A.R., "Computation of Blast Wave Encounter with Military Targets," Flow Simulations, Inc., Sunnyvale, Calif., Rept. No. 80-02, April 1980.

[14] Baldwin, B.S. and Lomax, H., "Thin Layer Approximation and Algebraic Model for Separated Turbulent Flow," AIAA Paper 78-257, Jan. 1978.

[15] Courant, R. and Friedrichs, K.O., *Supersonic Flow and Shock Waves,* Interscience Publishers, Inc., New York, 1948, pp. 329-331.